

Comparison of the dislocation density obtained by HR-EBSD and X-ray profile analysis

Szylvia Kalácska, István Groma, András Borbély, and Péter Dusán Ispánovity

Citation: *Appl. Phys. Lett.* **110**, 091912 (2017); doi: 10.1063/1.4977569

View online: <http://dx.doi.org/10.1063/1.4977569>

View Table of Contents: <http://aip.scitation.org/toc/apl/110/9>

Published by the [American Institute of Physics](#)

Articles you may be interested in

[Optical investigation of semi-polar \(11-22\) Al_xGa_{1-x}N with high Al composition](#)

Appl. Phys. Lett. **110**, 091102091102 (2017); 10.1063/1.4977428

[Direct observation of trapped charges under field-plate in p-GaN gate AlGaN/GaN high electron mobility transistors by electric field-induced optical second-harmonic generation](#)

Appl. Phys. Lett. **110**, 092101092101 (2017); 10.1063/1.4977084

[How predictable is plastic damage at the atomic scale?](#)

Appl. Phys. Lett. **110**, 091902091902 (2017); 10.1063/1.4977420

[Surface effects on the photoconducting properties of SrTiO₃ thin films](#)

Appl. Phys. Lett. **110**, 091103091103 (2017); 10.1063/1.4976944

[Thermal behavior and carrier injection of GaAs/GaP quantum dots light emitting diodes](#)

Appl. Phys. Lett. **110**, 091101091101 (2017); 10.1063/1.4977716

[Solid solution strengthening in GaSb/GaAs: A mode to reduce the TD density through Be-doping](#)

Appl. Phys. Lett. **110**, 092103092103 (2017); 10.1063/1.4977489

Fearful for the future of science?

Sign up for **FREE** FYI emails.
AIP American Institute of Physics

Comparison of the dislocation density obtained by HR-EBSD and X-ray profile analysis

Szilvia Kalácska,¹ István Groma,^{1,a)} András Borbély,² and Péter Dusán Ispánovity¹

¹Department of Materials Physics, Eötvös University Budapest, H-1517 Budapest POB 32, Hungary

²Ecole Nationale Supérieure des Mines, SMS-EMSE, CNRS:UMR 5307, LGF, 42023 Saint-Etienne Cedex 2, France

(Received 26 October 2016; accepted 15 February 2017; published online 2 March 2017)

Based on the cross-correlation analysis of the Kikuchi diffraction patterns, high-resolution electron backscatter diffraction (HR-EBSD) is a well established method for determining internal stress in the deformed crystalline materials. In many cases, however, the stress values evaluated at different sampling points have a large scatter of the order of GPa. As demonstrated by Wilkinson *et al.* [Appl. Phys. Lett. **105**, 181907 (2014)], this is due to the long tail of the probability distribution ($P(\sigma)$) of the eigenstress generated by the dislocations present in the system. According to the theoretical investigations of Groma and Bakó [Phys. Rev. B **58**, 2969 (1998)], the tail of $P(\sigma)$ is inverse cubic with a prefactor proportional to the total dislocation density $\langle \rho \rangle$. This paper presents the details of $\langle \rho \rangle$ determination from $P(\sigma)$ contributing to the proper physical understanding of the method. The $\langle \rho \rangle$ values determined on the deformed Cu single crystals show good agreement with the results of X-ray line profile analysis, granting credibility to the EBSD approach. The availability of spatially resolved stress maps opens further perspectives for the evaluation of correlation properties and mesoscale parameters of heterogeneous dislocation structures. *Published by AIP Publishing.* [<http://dx.doi.org/10.1063/1.4977569>]

The quantitative characterization of plastically deformed crystals in terms of dislocation density by transmission electron microscopy (TEM) and X-ray diffraction (XRD) was a very important step in the development of basic models of crystal plasticity.¹ This is especially true in the case of the composite model² of heterogeneous dislocation structures, which postulates a Taylor type³ relation between the local flow stress and local dislocation density. Accessing local field quantities, however, requires methods capable of capturing structural heterogeneities at the sub-micrometer scale, which can be obtained with the TEM, but gathering statistically significant information usually involves a large amount of manual work. Therefore, establishing automated characterization methods providing information on the dislocation density and other microstructural parameters at the meso-scale could be very useful for corroborating the continuum theories of plasticity developed during the last decade.⁴⁻⁷

It is the aim of the present work to explore the relevance and potential of the electron backscatter diffraction (EBSD) method based on the statistical properties of the local stress distribution determined by high-resolution electron backscatter diffraction (HR-EBSD).⁸ To address their physical significance, the results will be compared to the outcome of discrete dislocation dynamics simulations and X-ray diffraction (XRD) line profile analysis,⁹ a well established experimental technique for characterising dislocation structures. The detailed analysis of the peak shape allows determining major microstructural parameters, such as the coherent domain size, the dislocation density and its fluctuation. As shown by Groma *et al.*⁹⁻¹² in the so-called “strain broadening” setup,⁹ where the 3D intensity distribution is integrated over the plane perpendicular to the diffraction vector, the two leading terms of the asymptotic decay region of the X-ray intensity distribution $I(q)$ can be read as

$$I(q) = \frac{1}{\pi^2 d} \frac{1}{q^2} + \frac{\Lambda}{4\pi^2} \langle \rho \rangle \frac{1}{q^3}, \quad (1)$$

where d is the coherent domain size, $q = 2[\sin(\Theta) - \sin(\Theta_0)]/\lambda$, $\langle \rho \rangle$ is the average dislocation density and λ is the wavelength of the X-rays. Θ and Θ_0 are the half of the scattering angle and the Bragg angle, respectively. The parameter Λ is commonly given in the form $\Lambda = 2|\vec{g}|^2|\vec{b}|^2C_g/\pi$, where \vec{b} and \vec{g} are the Burgers and the diffraction vector, respectively. C_g is the *diffraction contrast factor* and it depends on the type of the dislocation and the relative geometrical position between the dislocation line direction and the direction of \vec{g} . A detailed description of the contrast factor calculation can be found in Ref. 13. It should be noted that the inverse cubic decay of the tail of $I(q)$ generated by the dislocations is the direct consequence of the $1/r$ type strain (stress) field developing around a dislocation. A remarkable feature of Eq. (1) is its independence from the configuration of dislocations usually described in terms of the dislocation-dislocation correlations. Certainly, the q value from which Eq. (1) describes well the asymptotic region depends on correlations, as it will be exemplified later. Since the tail of the experimental intensity curve can be rather noisy, the actual values of the coherent domain size and the dislocation density can be more accurately evaluated from the second order restricted moment defined as^{9,11}

$$M_2(q) = \frac{\int_{-q}^q q'^2 I(q') dq'}{\int_{-\infty}^{\infty} I(q') dq'}. \quad (2)$$

Analysing higher order restricted moments can also be useful;^{10,11} however, for the analysis presented here, the use of $M_2(q)$ is sufficient. After substituting Eq. (1) into Eq. (2) after large enough q values, we get

^{a)}Electronic mail: groma@metal.elte.hu

$$M_2(q) = \frac{1}{\pi^2 d} q + \frac{\Lambda}{2\pi^2} \langle \rho \rangle \ln\left(\frac{q}{q_0}\right), \quad (3)$$

where q_0 is a constant depending on the dislocation-dislocation correlation. If the coherent domain size is larger than of about $1 \mu\text{m}$, the first term in Eq. (3) is negligible besides the second one caused by the dislocations, and the plot of M_2 versus $\ln(q)$ becomes a straight line in the asymptotic regime $q \rightarrow \infty$. Its slope is proportional to the mean dislocation density. Using this feature, the dislocation density can be determined with an accuracy of a few percent.

HR-EBSD is a scanning electron microscope (SEM) based method, which allows determining the stress/strain in a crystalline material at the length scale of tens of nanometers. It is based on a cross-correlation method^{8,14–19} exploiting small changes in the backscattered Kikuchi diffraction patterns corresponding to a reference point and the actual point analysed. A detailed description of the technique can be found in Refs. 14 and 16. It was evidenced by Wilkinson *et al.*^{17–19} that local stress in a deformed polycrystalline material can be unexpectedly high and can vary by as much as ± 1 GPa. This unusual behavior is the consequence of the $1/r$ type long-range stress field generated by a dislocation. According to the analytical calculations of Groma *et al.*^{20,21} the tail of the probability distribution density of the internal stress generated by a set of straight parallel dislocations decays as

$$P(\sigma) \rightarrow G^2 |\vec{b}|^2 C_\sigma \langle \rho \rangle \frac{1}{\sigma^3}, \quad (4)$$

where G is the shear modulus and C_σ (in analogy with XRD) is defined as the *stress contrast factor* since its value depends on the type of dislocation, its line direction and the considered stress component σ_{ij} .²⁰ Similarly, to the X-ray line profile case, the tail of the probability distribution is affected not by the actual dislocation arrangement but only by the average number of dislocations crossing the unit surface. To demonstrate this, we took a set of 512 parallel edge dislocations with the Burgers vectors parallel to the horizontal axis. Initially, the dislocations were placed randomly in a square region, and then the system was relaxed with an overdamped dynamics (the velocity of a dislocation is proportional to the stress at the dislocation)²² using the periodic boundary conditions. For the initial and the relaxed configurations (Figs. 1(a) and 1(b)), the probability distribution of the shear stress was numerically determined by taking the stress values generated by the dislocation system at 10^6 randomly selected points. As shown in Fig. 1(c), the tail of the distribution is not affected by the relaxation (in agreement with the theoretical predictions^{20,21}), while the central region of $P(\sigma)$ becomes narrower in the relaxed state (inset in Fig. 1(c)). It is important to note that for a completely random dislocation distribution, the half width of $P(\sigma)$ tends to infinity with the logarithm of the system size, while for the relaxed configuration this divergence is canceled by the dislocation-dislocation correlations.²⁰ So, due to stress screening caused by the spatial correlations, the distribution $P(\sigma)$ becomes independent from the size of the system.²⁰ Similarly, to Bragg peak broadening, the tail of $P(\sigma)$ is inverse cubic in the asymptotic regime. Hence, its second order moment becomes

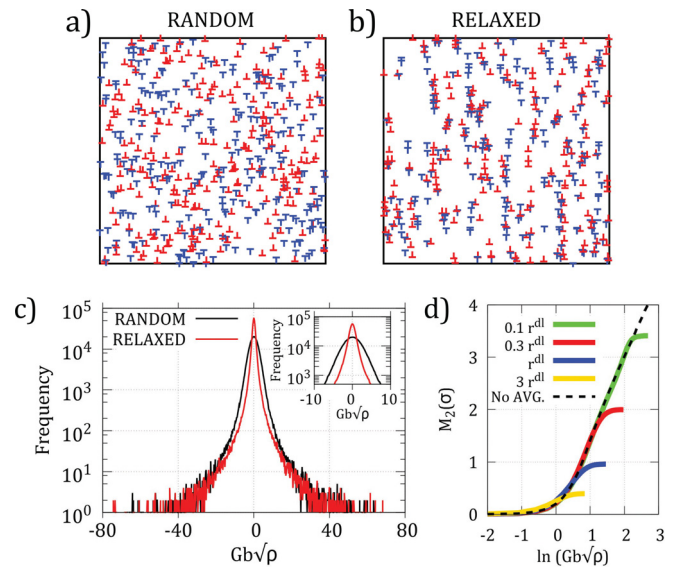


FIG. 1. (a) Random and (b) relaxed dislocation configuration. (c) Internal stress distributions obtained for the random (black curve) and the relaxed (red curve) configurations. In the inset, the central part of the distributions is enlarged. (d) The $M_2(\sigma)$ vs. $\ln(\sigma)$ for 4 different averaging box-sizes and without averaging corresponding to the relaxed configuration.

linear in $\ln(\sigma)$ with a slope proportional to the average dislocation density.

Due to the finite volume illuminated by the electrons in the SEM, a physically correct interpretation of experimental stress distributions requires averaging the theoretical distributions over the volume illuminated. This introduces a cut-off in the inverse cubic decay of $P(\sigma)$. As a consequence, the plot of M_2 versus $\ln(\sigma)$ deviates from the expected linear behavior, as demonstrated in Fig. 1(d), showing the second order restricted moments corresponding to four “spatially averaged distributions” calculated for circles with diameters equal to $0.1r^{\text{dl}}$, $0.3r^{\text{dl}}$, r^{dl} , and $3r^{\text{dl}}$, where r^{dl} is the average dislocation-dislocation distance. The curve without averaging is also shown. As expected, the stress level at the cut-off is decreasing with an increasing diameter or dislocation density. Therefore, during the evaluation of real data, the cut-off introduced by the finite beam size should be considered in the analysis. Since the characteristic linear size of the illuminated volume (of about $10 \times 10 \times 50 \text{ nm}^3$)^{23,24} can be of the same order of magnitude as the average dislocation-dislocation spacing in a heavily deformed metal (of $\approx 30 \text{ nm}$ for $\rho \approx 10^{15} \text{ m}^{-2}$), the finite beam size could become a limiting factor for the application of the method.

To check the reliability of the HR-EBSD method for dislocation density evaluation, subsequent analyses were done by HR-EBSD and XRD on the same crystal surfaces. The Cu single crystals of rotated Goss orientation (011)[01 $\bar{1}$] were cut by electrical discharge machining into cuboid shapes and deformed by channel die compression up to the strain levels of 6% and 10%. The compression was performed parallel to the [110] plane normal, while the sample elongated along the [1 $\bar{1}$ 0] direction, and it was held fixed by the channel walls along the [100] direction. Before deformation, HR-EBSD and XRD analyses, the samples were electropolished.

The rotated Goss orientation deforms homogeneously in channel die compression. According to the band contrast

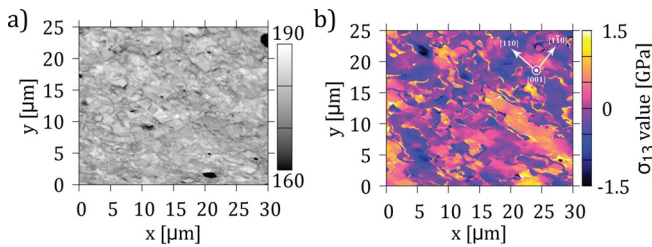


FIG. 2. (a) Band contrast map obtained on the sample deformed up to 6% strain. (b) The σ_{13} stress component map obtained by HR-EBSD on the same sample. The stress levels indicated are relative values to the stress level at the center of the scanned area.

map shown in Fig. 2(a), a well defined dislocation cell structure develops already at 6% with an average cell size of about 2–3 μm . (At 10% it is somewhat smaller.) The samples were then characterized by XRD by measuring the 200 line profile on the [100] surface. The measurements were done with Cu $K_{\alpha 1}$ radiation in a Panalytical MRD diffractometer equipped with a Bartels primary monochromator and a double bounce analyser, both made of Ge.

The 200 peaks and their variances $M_2(q)$ versus $\ln(q)$ are shown in Figs. 3(a) and 3(b), respectively. The dislocation density is directly obtained from the slope of the lines fitted to the asymptotic regime. The results given in the second column of Table I were obtained using a diffraction contrast factor $C_g = 0.397$ corresponding to an equal dislocation population in each slip system.

The EBSD scans were done with a step size of 100 nm on a square grid covering an area of 25 $\mu\text{m} \times 30 \mu\text{m}$. The backscattered Kikuchi patterns were recorded with a NordlysNano detector of 1344 \times 1024 pixels. The acquisition was monitored with the AztecHKL software, which was also used to calculate the pattern centers necessary for performing the high-resolution evaluation. The stress at each measurement point was determined with the cross-correlation method of the Kikuchi patterns proposed by Britton and Wilkinson.¹⁶ Since the scanned area is much larger than the characteristic size of the microstructure (dislocation cells with a size of about 1 μm , see Fig. 2(a)), the probability distribution of internal stresses can be considered as a macroscopic quantity characterizing the structure.

The σ_{13} stress component map obtained on the sample with 6% strain is plotted in Fig. 2(b). In agreement with the band contrast map (Fig. 2(a)), the cell structure with typical cell size of 2–3 μm is shown, where long range internal stress

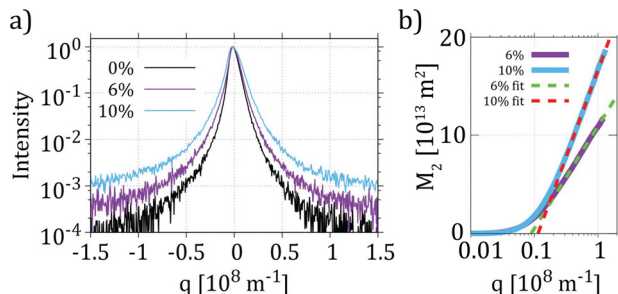


FIG. 3. (a) 200 X-ray Bragg peaks corresponding to 0%, 6%, and 10% strain. (b) The variance M_2 vs. $\ln(q)$ of the peaks measured on the deformed samples. The straight lines are fits to the asymptotic regime.

TABLE I. Total dislocation densities obtained by X-ray line profile analysis and HR-EBSD together with the density of geometrically necessary dislocations (GND) determined from HR-EBSD.

Strain	ρ_{XRD} (m^{-2})	ρ_{EBSD} (m^{-2})	ρ_{GND} (m^{-2})
6%	7.3×10^{14}	2.3×10^{14}	1.4×10^{14}
10%	1.2×10^{152}	1.3×10^{15}	2.5×10^{14}

develops in the cell interiors.² The band contrast and the stress maps are rather similar for the sample deformed up to 10% strain, but the cell size is smaller of about 1–2 μm .

The probability distributions of the σ_{13} stress component characterizing the undeformed and deformed samples are plotted in Fig. 4(a). $P(\sigma_{13})$ is very narrow for the undeformed sample, and it broadens with increasing deformation. Remarkably, the tails of $P(\sigma_{13})$ extend outside values as large as ± 1 GPa. Similar behavior was first reported by Wilkinson *et al.* on the deformed polycrystalline Cu and ferritic steel.¹⁹ Since one can clearly identify a linear regime on the M_2 versus $\ln(\sigma_{13})$ plots (Fig. 4(b)), the broadening of $P(\sigma_{13})$ can only be caused by the presence of dislocations (other type of stress source would generate different decay in the tail part²⁰). This reasoning is also supported by the rather narrow $P(\sigma_{13})$ distribution corresponding to the undeformed sample. For stress values larger than about 2 GPa, the second order restricted moments clearly deviate from the linear dependence in $\ln(\sigma_{13})$. As discussed above, this is the consequence of the measuring setup and related to the unavoidable averaging over the volume illuminated by the electron beam. Nevertheless, the linear regime can be well identified on the plots presented. (The cut-off is certainly absent on the variance of the X-ray peaks.) According to Fig. 1(d), the linear region disappears when the size of the averaging zone equals the mean dislocation-dislocation spacing. This imposes an instrumental limit in the application of the method for heavily deformed samples.

According to Eq. (4), the slope of the line fitted in the asymptotic regime is proportional to the total dislocation density. Its determination requires the knowledge of the stress contrast factor C_σ in Eq. (4), which can be calculated according to Refs. 20 and 21. For the stress component σ_{ij} considered in the analysis, one has to evaluate the integral

$$C_{\sigma_{ij}} = \frac{1}{G^2 |b|^2} \int_0^{2\pi} [r \sigma_{ij}^{\text{ind}}(r, \varphi)]^2 d\varphi, \quad (5)$$

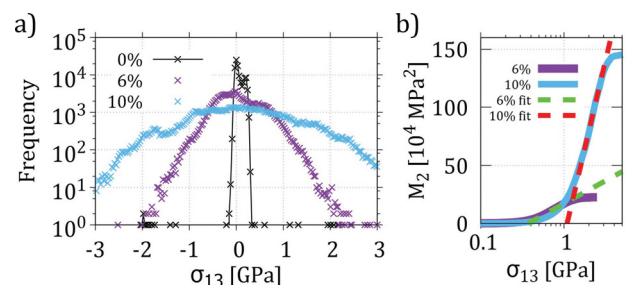


FIG. 4. (a) The probability distribution of the σ_{13} component at strains of 0%, 6% and 10%. (b) The corresponding variances M_2 versus $\ln(\sigma_{13})$ for the deformed samples, with the straight lines fitted to the asymptotic regime.

where σ_{ij}^{ind} is the stress generated by a dislocation with a given line direction \vec{l} and Burgers vector \vec{b} in the xy plane of the coordinate system, in which the stress tensor is calculated during the evaluation of the Kikuchi patterns. In Eq. (5), (r, φ) denotes the polar coordinates in the xy plane. (Due to the $1/r$ type of decay of the stress field generated by a dislocation, the integral is independent of r .) Since in anisotropic materials the stress field of a straight dislocation cannot be always given in a closed analytical form,²⁵ C_σ can only be calculated numerically. Moreover, since in most cases dislocations of different types and line directions can exist in the same structure, one has to calculate the appropriate weighted average of C_σ corresponding to given \vec{b} and \vec{l} . This issue is out of the scope of this paper. For simplicity, we use the value corresponding to an edge dislocation with line direction perpendicular to the sample surface. In this case, $C_\sigma = 1/(8\pi(1-\nu)^2)$ where ν is the Poisson number.²⁰

The dislocation densities of the deformed samples are summarized in the third column of Table I. The ρ_{EBSD} values given correspond to the average values obtained from the stress components σ_{13} , σ_{22} , and σ_{23} . (Due to the deformation geometry applied, the other two stress components σ_{11} and σ_{12} are much smaller with much larger error, so they were not taken into account.) For comparison, the geometrically necessary dislocation density (GND) is also determined from the α_{i3} components of the Nye's dislocation density tensor accessible by EBSD.^{26,27} As expected, the GND density is always smaller than the statistically stored one. The values for the latter obtained by XRD or HR-EBSD are in acceptable agreement. At 10% strain, the difference is within a few % of relative error, while at 6% strain the HR-EBSD gave smaller ρ than the XRD by about a factor of 3. The last difference can be attributed first of all to the influence of the larger dislocation cell size at 6% strain, resulting that the volume scanned during the EBSD measurement may not be large enough to give a representative mean value for the dislocation density. Another reason for the difference can be a change in the main dislocation character and the population of different slip systems with increasing strain. It seems that the C_σ used is not really relevant for the 6% strain case. The issue requires further detailed investigations. However, it is remarkable that the assumption considering only edge dislocations gave good agreement with the XRD results at 10% strain. This emphasizes the strong physical basis of the proposed evaluation method.

Since, however, HR-EBSD provides maps, like stress, GND, and orientation, one can determine microstructural parameters characterizing the spatial distribution of the dislocations that are crucial for physically based plasticity modeling. To demonstrate this potential of HR-EBSD, the autocorrelation function (ACF) of the σ_{13} stress component obtained on the two deformed samples is provided (Fig. 5). As it is shown in Fig. 5(b), the stress ACFs have an elliptical symmetry and they decay as $\sim \ln(r/r_0(\phi))$ (Fig. 5(c)), where the length scale parameter r_0 depends on the polar angle ϕ . This means the dislocation-dislocation correlation function decays faster than a power law,²⁸ but the correlation length corresponding to r_0 is rather large (several μm) and in contrast to the cell size it is increasing with deformation. This finding seems to contradict with the principle of similitude,

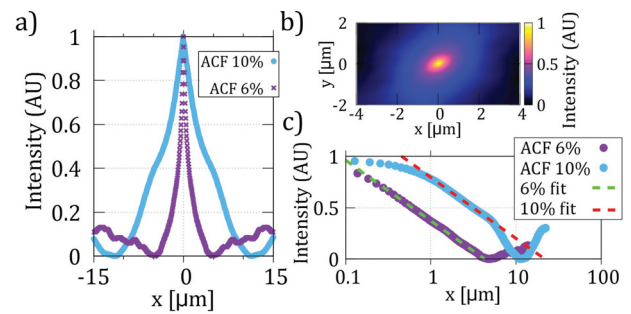


FIG. 5. (a) Line plots along the x axis of the 2D autocorrelation functions of the σ_{13} stress component map measured on the deformed samples. (b) The central part of the 2D autocorrelation function of σ_{13} measured at 6% strain. (c) The semilogarithmic plots indicating the logarithmic asymptotic decay of the stress autocorrelation.

but since the “long-range” stress autocorrelation is generated by the GND walls, the evolution of their spatial arrangement can lead to increasing autocorrelation length scale. As it is found, the ratio of the GND and stored dislocation densities are not constant (see Table I), so there are two “separate” length scales in the system. More detailed analyses will be published elsewhere.

In sum, HR-EBSD was traditionally used to determine the *GND density*.^{26,27,29} With the analysis of the tail of the stress probability-distribution function obtained from HR-EBSD, the stored, *total dislocation density* present in the sample can also be determined. Furthermore, analysing the statistical properties of the different quantities, like stress and GND maps, opens further perspectives for the application of HR-EBSD in determining *mesoscale* parameters of heterogeneous samples. These parameters are crucial for validating the continuum theory of dislocations proposed during the past decade.⁴⁻⁷

The authors acknowledge the insightful discussion with Dr. Claire Maurice (Ecole Nationale Supérieure des Mines, Saint-Etienne, France). This work was supported by the French-Hungarian collaboration BALATON, the Hungarian Scientific Research Fund (OTKA) under Contract Nos. K-105335 and PD-105256, and the European Commission under Grant Agreement No. CIG-321842. PDI was supported by the János Bolyai Scholarship of the Hungarian Academy of Sciences, No. BO/880/15.

¹H. Mughrabi and T. Ungar, *Dislocations in Solids* (Elsevier, 2002), Vol. 11.

²T. Ungar, H. Mughrabi, D. Rönnpagel, and M. Wilkens, *Acta Metall.* **32**, 333 (1984).

³G. I. Taylor, *Proc. R. Soc. London, Ser. A* **145**, 362 (1934), ISSN 0950-1207.

⁴A. El-Azab, *Phys. Rev. B* **61**, 11956 (2000).

⁵I. Groma, F. Csikor, and M. Zaiser, *Acta Mater.* **51**, 1271 (2003), ISSN 1359-6454.

⁶T. Hochrainer, M. Zaiser, and P. Gumbsch, *Philos. Mag.* **87**, 1261 (2007), ISSN 1478-6435.

⁷M. Zaiser, *Phys. Rev. B* **92**, 174120 (2015).

⁸A. Wilkinson, E. Clarke, T. Britton, P. Littlewood, and P. Karamched, *J. Strain Anal. Eng. Des.* **45**, 365 (2010).

⁹I. Groma, *Phys. Rev. B* **57**, 7535 (1998).

¹⁰F. Székely, I. Groma, and J. Lendvai, *Phys. Rev. B* **62**, 3093 (2000).

¹¹A. Borbély and I. Groma, *Appl. Phys. Lett.* **79**, 1772 (2001).

¹²I. Groma, D. Tüzes, and P. Ispánovity, *Scr. Mater.* **68**, 755 (2013).

- ¹³A. Borbély, J. Dragomir-Cernatescu, G. Ribárik, and T. Ungár, *J. Appl. Cryst.* **36**, 160 (2003).
- ¹⁴A. J. Wilkinson, G. Meaden, and D. J. Dingley, *Ultramicroscopy* **106**, 307 (2006).
- ¹⁵A. Wilkinson, T. Britton, J. Jiang, G. Meaden, and D. Dingley, *Microsc. Microanal.* **17**, 402 (2011).
- ¹⁶T. Britton and A. Wilkinson, *Ultramicroscopy* **114**, 82 (2012).
- ¹⁷J. Jiang, T. B. Britton, and A. J. Wilkinson, *Acta Mater.* **61**, 5895 (2013).
- ¹⁸J. Jiang, T. B. Britton, and A. J. Wilkinson, *Acta Mater.* **94**, 193 (2015).
- ¹⁹A. J. Wilkinson, E. Tarleton, A. Vilalta-Clemente, J. Jiang, T. B. Britton, and D. M. Collins, *Appl. Phys. Lett.* **105**, 181907 (2014).
- ²⁰I. Groma and B. Bakó, *Phys. Rev. B* **58**, 2969 (1998).
- ²¹F. F. Csikor and I. Groma, *Phys. Rev. B* **70**, 064106 (2004).
- ²²P. D. Ispánovity, I. Groma, G. Györgyi, F. F. Csikor, and D. Weygand, *Phys. Rev. Lett.* **105**, 085503 (2010).
- ²³N. Yao and Z. Wang, *Handbook of Microscopy for Nanotechnology, Nanostructure Science and Technology Series* (Springer US, 2006), ISBN 9781402080067.
- ²⁴D. Chen, J. Kuo, and W. Wu, *Ultramicroscopy* **111**, 1488 (2011), ISSN 0304-3991.
- ²⁵J. W. Steeds, *Introduction to Anisotropic Elasticity Theory of Dislocations* (Clarendon Press, 1973).
- ²⁶B. El-Dasher, B. Adams, and A. Rollett, *Scr. Mater.* **48**, 141 (2003).
- ²⁷W. Pantleon, *Scr. Mater.* **58**, 994 (2008).
- ²⁸M. Zaiser and A. Seeger, “Long-range internal stresses, dislocation patterning and work-hardening in crystal plasticity,” in *Dislocations in Solids* (Elsevier, 2002), Vol. 11, Chap. LVI, pp. 1–100.
- ²⁹A. J. Wilkinson and D. Randman, *Philos. Mag.* **90**, 1159 (2010).